Macromolecules

ARTICLE

pubs.acs.org/Macromolecules

Exciplex Electroluminescence Induced by Cross-Linked Hole-Transporting Materials for White Light Polymer Light-Emitting Diodes

Yen-Ju Cheng,* Ming-Hung Liao, Hung-Min Shih, Ping-I Shih, and Chain-Shu Hsu

Department of Applied Chemistry, National Chiao Tung University, 1001 Ta Hsueh Road, Hsin-Chu, 30010 Taiwan

Supporting Information

ABSTRACT: A new class of cross-linkable *N*,*N*,*N*′,*N*′-tetraphenyl-1,1′-biphenyl-4,4′-diamine (TPD)-based hole-transporting materials (HTMs), **DV-OMe-TPD**, **DV-Me-TPD**, and **DV-F-TPD**, were designed and synthesized. Two vinyl groups in the TPD units are used for thermal cross-linking, whereas methoxy, methyl and fluoro groups are introduced to modulate the HOMO energy levels of the HTMs. These HTMs are thermally cross-linked to overcome interfacial mixing, realizing solution-processed polyfluorene (PFO)-based devices (ITO/cross-linked HTMs/PFO/CsF/Al). Besides the characteristic blue emission of PFO, the devices exhibited a red emission whose energy is highly dependent on the HOMO energy of the cross-linked HTM used in the device. This result suggests that the red electroluminescence is derived from the exciplex generated by the adjacent hole and electron at the cross-linked HTM/fluorenone heterojunction interface. By doping small amount of 4,7-bis(9,9-dihexylfluoren-2-yl)-2,1,3-benzothiadiazole (**BFBT**) into the emissive layer (EML) to compensate green emission, the devices with the configuration of ITO/PEDOT:PSS/**DV-Me-TPD**/PFO doped with **BFBT**/CsF/Al exhibited white electroluminescence comprising three primary colors simultaneously. The 0.04 wt % doped device achieved a maximum luminous efficiency of 5.28 cd/A, which represents the highest efficiency for WPLEDs reported so far on the basis of the exciplex strategy. This device showed CIE chromaticity coordinates of (0.32, 0.42) which are close to the ideal white point (0.33, 0.33). We have demonstrated that integrating cross-linked triarylamine-based HTMs with fluorenone defects in PFO to induce exciplex electroluminescence can provide a useful way for realizing WPLED devices.

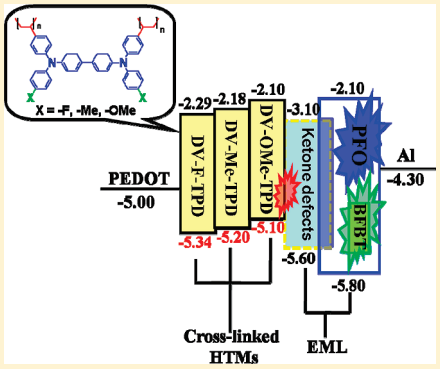

INTRODUCTION

White light-emitting diodes (WLEDs) have received considerable interest due to their potential applications in full color flat panel displays, back-lighting sources for liquid-crystal displays, and solid-state lighting sources.[1] White polymer light-emitting diodes (WPLEDs) are particularly promising, because polymer-based devices possess several advantages such as low cost, flexibility and large area by solution processing.[2] A ideal white PLED is characterized by an emission that covers the full spectral range of the visible region (380−780 nm) and a Commission International d'Eclairage (CIE) chromaticity coordinates of (0.33, 0.33). To create white-light emission, the most straightforward way is to mix three components which can independently emit three primary colors (red, green, and blue). Several strategies have been implemented to realize WPLEDs by blending three emitting components such as polymer blends[3] or polymers doped with small molecules.[4] However, severe phase separation or undesired energy transfer between different components are critical issues to control the color composition.[5] Single-polymer systems with different chromophoric groups on the main chain or side chain have been reported to address this problem.[6] It is highly desirable to develop other emissive systems that can reduce the number of emissive components to achieve white light electroluminescence.

To achieve high-performance LEDs devices, triarylamine-based hole transporting layers (HTL) are widely incorporated into multilayer devices to improve the hole transporting properties.[7] Because of their relatively high-lying LUMO energy levels, these HTLs also function as effective electron-blocking layers to confine electrons in the emissive layer (EML) near the interface with HTL. When the electron and hole recombine in the EML, exciton emission with pure emissive band will be observed. If the electron is confined in the EML, while the hole is still located in the HTL, the transient bimolecular excited state, also termed as exciplex, can be formed by adjacent hole and electron at the HTL/EML heterojunction interface.[8] Exciplex usually results in a characteristic broad and structureless emission. In addition, compared to the exciton emission coming from a single species (i.e., EML or HTL material), the exciplex emission is bathochromically shifted to the longer wavelengths, because its energy is associated with the energy offset between the HOMO of the HTL material and the LUMO of the EML material. The occurrence of the undesired exciplex emission is detrimental to a PLED device that requires single-color

Received: March 26, 2011
Revised: June 13, 2011
Published: July 11, 2011

Scheme 1. Chemical Structures of the Cross-Linkable HTMs and Green Dope Material BFBT

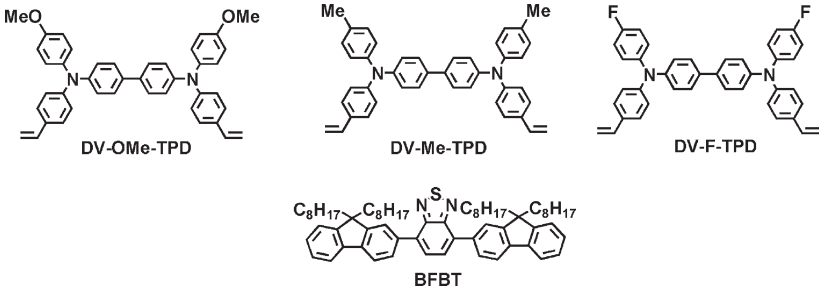

Scheme 2. Synthesis of Cross-Linkable HTMs

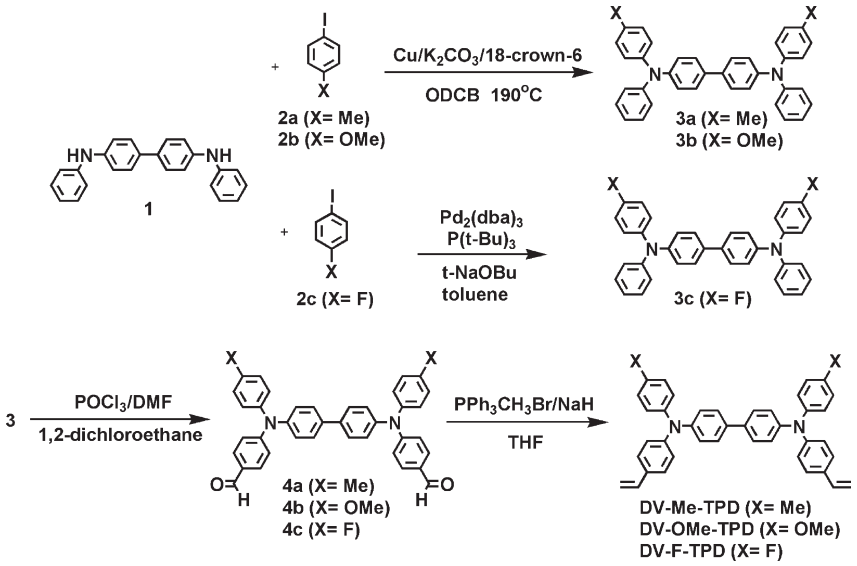

illumination. However, if this additional emission can be smartly controlled and utilized, it may provide a suitable red-light emission in the visible region for WPLED. Modulating electronic properties of the hole-transporting material affords a promising way to tailor the exciplex characteristics and its emission. Nevertheless, bilayer exciplex emission at HTL/EML interface is not well exploited for polymer-based WLEDs, and the performance based on this strategy in the literatures is still limited. The major obstacle to hinder this direction is that the bottom hole-transporting layer will be eroded by the solvent used in the subsequent spin-coating to deposit the emissive layer.[9] In this case, hole will be trapped at interfacial mixing zone near the heterojunction.[10] Therefore, incorporation of various hole-transporting materials to realize WPLEDs by exciplex strategy is technologically difficult. Until now, only poly(vinyl carbazole) (PVK) having certain solvent resistance represents the most commonly used HTM for multilayer devices.[11] Jen and coworkers have reported a series of triarylamine-based hole-transporting materials attaching two additional styrene groups for thermal cross-linking.[12] These small-molecule-based HTMs can be *in situ* converted into solvent-resistant, cross-linked networks, so that interfacial mixing can be overcome to realize multilayer devices by all-solution processing. However, the extra functionality used for cross-linking purpose is insulating moiety that will deteriorate hole transportation.[12a] We envisaged that the hole-transporting properties can be further improved if the insulating portion can be minimized. On the basis of this consideration, we have designed a new class of thermally cross-linkable hole-transporting materials based on the most widely used small molecule, *N*,*N*,*N*′,*N*′-tetraphenyl-1,1′-biphenyl-4,4′-diamine (TPD).[13] Two vinyl groups are directly introduced on the two phenyl rings in the TPD unit, forming two styrene groups to serve as the cross-linkers.[14] This molecular design creates the most compact HTM hybridizing TPD and styrene units together, which significantly increases the weight content of active TPD unit. Moreover, in order to fine-tune the electronic properties of HTMs, the *para* position of the other two phenyl rings in the TPD is further introduced with strong electron-donating methoxy groups (denoted as **DV-OMe-TPD**), weak electron-donating methyl group (denoted as **DV-Me-TPD**) and electron-withdrawing group (denoted as **DV-F-TPD**). Their molecular structure is shown in Scheme 1.

Polyfluorenes (PFO) have been demonstrated as a good candidate for blue PLEDs because of their high photoluminescence (PL) quantum efficiency.[15] However, the blue-light emitting devices based on homopolymer PFO suffer from the poor color stability due to the formation of fluorenone defects.[16] It is envisaged that this unwanted fluorenone impurity in PFO for blue PLEDs can become utilizable for WPLEDs. On the basis of the newly designed cross-linkable HTMs toward WPLEDs in this

dx.doi.org/10.1021/ma2006969 |*Macromolecules* 2011, 44, 5968–5976

Table 1. Physical Properties of the HTMs

HTMs	T_d[a] (°C)	T_c[b] (°C)	λ_{max} (nm)[c] uncross-linked	λ_{max} (nm)[d] cross-linked	HOMO[e] (eV)	E_g[f] (eV)	LUMO[g] (eV)
DV-TPD-OMe	448	168	377	363	−5.10	3.00	−2.10
DV-TPD-Me	462	147	372	359	−5.20	3.02	−2.18
DV-TPD-F	454	106	367	351	−5.34	3.05	−2.29

[a] T_d is the decomposition temperature determined by TGA at 5% weight loss. [b] T_c is the temperature of maximum exothermic peak obtained from DSC. [c] The wavelength of maximum absorption before cross-linking of HTMs. [d] The wavelength of maximum absorption of HTMs after cross-linking. [e] HOMO energy level was calculated by CV using ferrocene value of −4.8 eV below the vacuum level. [f] E_g^{opt} is the optical band gap. [g] LUMO = HOMO + E_g^{opt}.

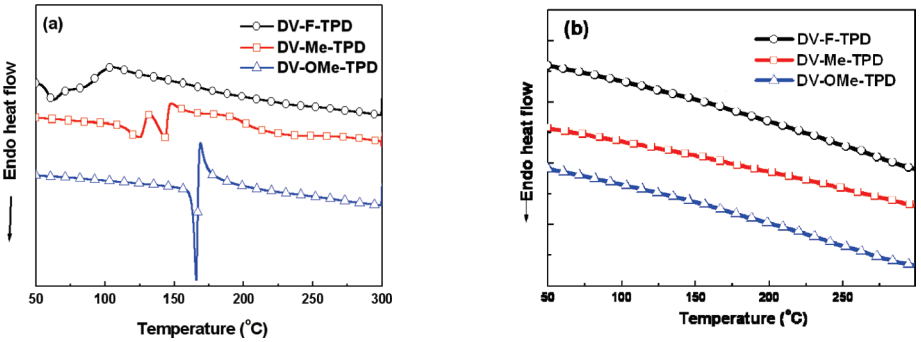

Figure 1. First heating (a) and second heating (b) of DSC measurements of the HTMs with a heating rate of 10 °C/min.

research, PFO is used to serve as the host to produce the blue emission, while the green emission is generated from a guest material, 4,7-bis(9,9-dihexylfluoren-2-yl)-2,1,3-benzothiadiazole (**BFBT**),[6c] doped into the EML (Scheme 1). The red emission comes from the exciplex formed at the interface between the cross-linked TPD-based molecule and the fluorenone species. By tuning the amount of **BFBT**, we have achieved white electroluminescence comprising the three primary colors simultaneously by blending only two components in the EML. Combining fluorenone defects in PFO with cross-linked HTMs to induce exciplex emission may afford an easy and useful strategy to achieve WPLEDs.

■ RESULTS AND DISCUSSION

Synthesis of Materials. The synthesis of these cross-linkable hole transporting materials are shown in Scheme 2. By utilizing Ullmann coupling, *N, N′*-diphenylbenzidine **1** was coupled with 2 equiv of 4-iodotoluene and 4-methoxyiodobenzene to yield TPD-based compound **3a** and **3b**, respectively, whereas **3c** was obtained by reacting **1** with 1-fluoro-4-iodobenzene by Hartwig−Buchwald palladium-catalyzed amination. Vilsmeier formylation of compound **3** with 2 equiv of phosphorus oxychloride ($POCl_3$) and *N,N*-dimethylformamide (DMF) to yield compound **4** after hydrolysis. Finally, the two formyl groups in the compound **4** were converted into two vinyl groups by using Wittig reaction to yield the corresponding cross-linkable HTMs **DV-Me-TPD**, **DV-OMe-TPD**, and **DV-F-TPD**.

Thermal Properties and Cross-Linking Conditions. The decomposition temperature (T_d) of the HTMs was determined by thermogravimetric analysis (TGA). All the HTMs showed high thermal stability with T_d ranging from 448 to 462 °C (Table 1). Differential scanning calorimetry (DSC) was used to investigate the thermal and cross-linking properties of these HTMs (Figure 1). In the first scan of DSC, all of the HTMs showed a board exothermic peak which is unambiguously indicative of the occurrence of cross-linking of styrene groups. It is noteworthy that the maximum exothermic temperature T_c follows the trend: **DV-F-TPD** (106 °C) < **DV-Me-TPD** (147 °C) < **DV-OMe-TPD** (168 °C). It has been generally accepted that two styrene groups undergo Diels−Alder dimerization followed by hydrogen radical transfer to generate the benzylic radical that initiates the vinyl radical polymerization.[14] The stability of benzylic radical intermediate will determine how easily the thermal cross-linking can occur. We propose that the electron-withdrawing ability of the *para* fluoro group reduces the electron density of nitrogen, thus improving the stability of benzylic radical, whereas methoxy group may decrease the radical stability. This electronic effect also permits us to fine-tune the cross-linking temperatures in the solid state. To prepare the thin film of these HTMs, 1.0 wt % chlorobenzene solutions of the HTMs were spin-coated onto the ITO substrate. On the basis of the DSC studies, we employed an isothermal heating at 180 °C for 30 min under nitrogen atmosphere to ensure complete cross-linking for all the HTMs.

Optical Properties and Solvent Resistance. The UV−vis absorption spectra of these HTMs in the solid film are shown in Figure S1 in the Supporting Information. **DV-OMe-TPD** showed the most red-shifted absorption maximum at 377 nm, whereas **DV-F-TPD** exhibited the most blue-shifted absorption maximum at 367 nm (Table 1). This can be rationalized by the fact that the electron-donating methoxy group raises the HOMO energy level, whereas the withdrawing fluoro group will lower the HOMO energy level. Compared with the uncross-linked HTMs in the solid state, the absorption maxima of the cross-linked HTMs are slightly blue-shifted presumably due to the disrupted coplanarity of TPD molecule after the covalent bonds are formed intermolecularly (Figure S1, Supporting Information). The resultant films are very transparent and absorb mainly in the UV region so it causes very little interference with the light generated from the device.

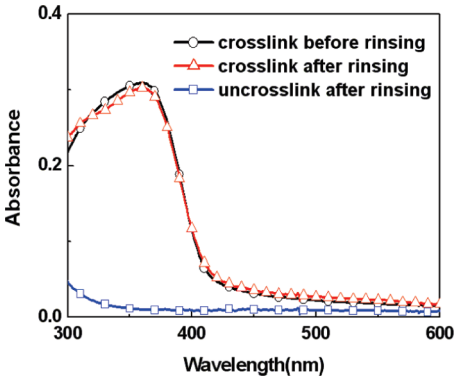

Figure 2. Absorption spectra of cross-linked **DV-Me-TPD** before washing and after washing by chlorobenzene, and un-cross-linked **DV-Me-TPD** absorption after washing.

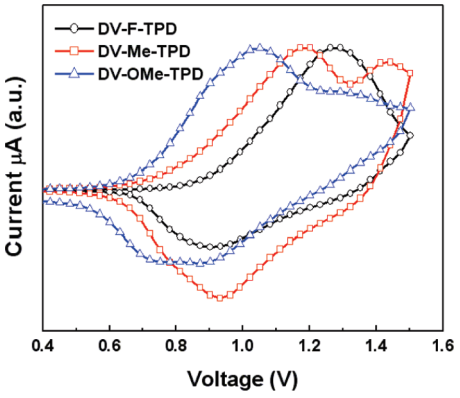

Figure 3. Cyclic voltammograms of the cross-linked HTMs on ITO in a solution of $(n\text{-}Bu_4)NBF_4$ in acetonitrile (0.1 M) at a scan rate of 100 mV/s.

Solvent resistance of the cross-linked HTMs was investigated by monitoring UV−vis spectra. As shown in Figure 2, the absorption intensity of the cross-linked **DV-Me-TPD** remains almost unchanged before and after rinsing with chlorobenzene (a good solvent for both precursor monomers and polyfluorene), indicating the sufficient solvent resistance has been generated. Similar phenomena were observed for **DV-OMe-TPD** and **DV-F-TPD**.

Furthermore, we employed Infrared spectroscopy to monitor the functional groups transformation. The vibrational stretching of the vinyl groups at 1627 cm^{-1} in **DV-Me-TPD** almost disappear after curing at 180 °C for 30 min, confirming that the solvent resistance comes from the cross-linking of the styryl groups (Figure S2, Supporting Information).

The surface roughness of the HTMs spin-coated on ITO was examined by atomic force microscopy (AFM) before and after thermal curing at 180 °C for 30 min (Figure S3, Supporting Information). Although these HTMs are small molecules, smooth and uniform thin films could be observed for each sample over a 2 × 2 μm scan area, and the root-mean-square (rms) surface roughness for **DV-Me-TPD**, **DV-F-TPD**, and **DV-OMe-TPD** is 0.37, 0.45, and 0.34 nm, respectively. After cross-linking, the surface roughness increased to 1.15, 1.00, and 0.97 nm for cross-linked **DV-Me-TPD**, **DV-F-TPD**, and **DV-OMe-TPD**, respectively. These results indicated that these small-molecule-based HTMs can have good film-forming properties.

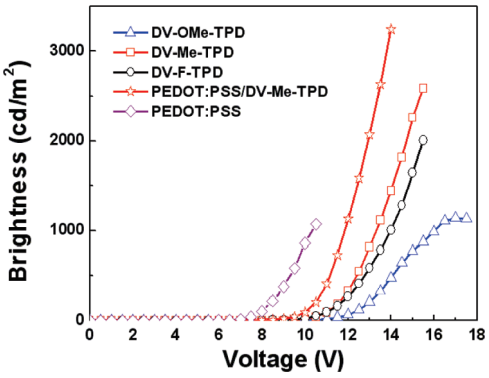

Figure 4. Brightness-voltage (B−V) characteristics based on the devices ITO/PEDOT:PSS/PFO/CsF/Al, ITO/HTMs/PFO/CsF/Al and ITO/PEDOT:PSS/**DV-Me-TPD**/PFO/CsF/Al.

Electrochemical Properties. Cyclic voltammetry (CV) was used to investigate the electrochemical properties of these hole transporting materials after these HTMs were cured at 180 °C for 30 min on the ITO (Figure 3). The highest occupied molecular orbital (HOMO) energy levels of these HTMs were estimated from the onset of oxidation potential using ferrocene/ferrocenium as standard, while the lowest unoccupied molecular orbital (LUMO) levels were estimated from the difference between the HOMO energy level and the optical band gap measured from absorption spectrum. Because the fluoro group with electron-withdrawing ability reduces the electron density of nitrogen, **DV-F-TPD** becomes more difficult to be oxidized and thus shows the lowest-lying HOMO energy level of −5.34 eV. As the electron-donating power of the substituent increases to strengthen the nitrogen electron density, the HOMO energy level gradually decreases to −5.20 for **DV-Me-TPD** and −5.10 eV for **DV-OMe-TPD**, respectively.

Device Performance. To estimate the intrinsic hole mobilities of these cross-linked HTMs, hole-only devices (ITO/PEDOT:PSS/cross-linked HTMs/Au) were first fabricated by means of the space-charge limit current (SCLC) theory. The device based on **DV-F-TPD**, **DV-Me-TPD**, and **DV-OMe-TPD** exhibited the comparable hole mobilities of 7.2×10^{-4} $cm^2/(V\,s)$, 6.2×10^{-4} $cm^2/(V\,s)$, and 3.4×10^{-4} $cm^2/(V\,s)$, respectively. To further investigate the hole-transporting properties of these new materials, we fabricated the devices with the configuration ITO/cross-linked HTMs/PFO/CsF/Al where PFO was employed as the blue emitting layer. The brightness-voltage ($L-V$) and luminous efficiency−current density characteristics of the device are shown in Figure 4 and Figure 5, respectively. Table 2 lists the device parameters. Compared to the devices with **DV-F-TPD** and **DV-OMe-TPD** as HTL, the device based on **DV-Me-TPD** exhibited the highest performance in terms of the lower operational voltage, higher maximum luminous efficiency (1.3 cd/A), and higher maximum brightness (2586 cd/m^2 at 15.5 V). Because the three HTMs have very similar molecular structures, the variations in device performance are presumably ascribed to the difference in HOMO energy levels. The work function of the ITO and the HOMO level of the PFO are located at −4.8 eV and −5.8 eV, respectively. The results suggest that **DV-Me-TPD** with the HOMO energy at −5.2 eV serves as the most suitable energy intermediate to provide a cascade hole-transporting

dx.doi.org/10.1021/ma2006969 |*Macromolecules* 2011, 44, 5968–5976

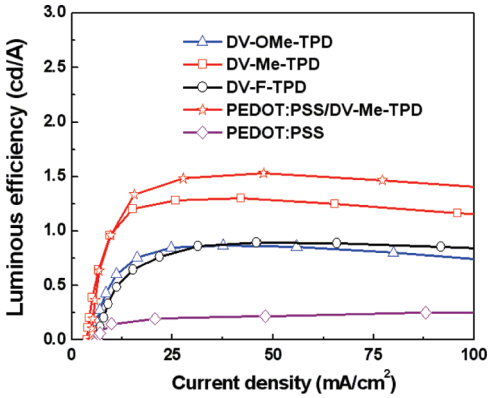

Figure 5. Luminous efficiency-current density characteristics based on the devices ITO/PEDOT:PSS/PFO/CsF/Al, ITO/HTMs/PFO/CsF/Al, and ITO/PEDOT:PSS/**DV-Me-TPD**/PFO/CsF/Al.

Table 2. Electroluminescence Data of Devices Based on the Structure (ITO/HTMs/PFO/CsF/Al)

HTMs	B^a (cd/m^2)	LE^a (cd/A)	B_{max} (cd/m^2)	LE$_{max}$ (cd/A)
PEDOT:PSS	39 (at 7.5 V)	0.19	1071 (at 10.5 V)	0.28
DV-OMe-TPD	161 (at 12.7 V)	0.79	1138 (at 17 V)	0.87
DV-F-TPD	148 (at 11.4 V)	0.73	2011 (at 15.5 V)	0.89
DV-Me-TPD	250 (at 12 V)	1.24	2586 (at 15.5 V)	1.30
PEDOT:PSS/ **DV-Me-TPD**	282 (at 10.7 V)	1.39	3245 (at 14 V)	1.53

[a] Recorded at 20 mA/cm^2.

pathway which allows for more balanced charge carriers in the devices. Raising (**DV-OMe-TPD**) or lowering (**DV-F-TPD**) the HOMO levels will also increase the energy barriers at **DV-OMe-TPD**/PFO (0.7 eV) or ITO/**DV-F-TPD** (0.54 eV) interfaces, respectively, thus resulting in unbalanced charge transportation and lower device performance. It should be noted that the devices incorporating these HTMs show much improved performance compared to a control device (ITO/PEDOT:PSS/PFO/CsF/Al) using PEDOT:PSS as hole-injection layer. The maximum luminous efficiency of the device with **DV-Me-TPD** is about 4 times higher than that of the device using PEDOT:PSS. This pronounced improvement in device performance is due to the balanced charge injection and transporting characters, leading to the effective charge recombination within the emitting layer.

In addition to the characteristic emission of PFO from 400 to 500 nm being observed in the electroluminescent spectra, the devices incorporating these cross-linked HTMs also showed a broad emission covering from 550 to 700 nm (Figure 6). It has been known that, under the thermal and electrical field circumstances, fluorene moieties in the PFO are prone to be oxidized to fluorenone species.[17] We speculate that this red emission may come from the exciplex at the interface between the fluorenone defects and HTL. Fortunately, these HTMs having different HOMO energy levels allow us to specifically investigate the origin of the red emission. It was found that the energy gap of 2.0 eV between the HOMO level of **DV-OMe-TPD** (−5.1 eV) and the LUMO level of fluorenone (−3.1 eV)[17] perfectly matches the energy of the red emission band (λ_{max} = 620 nm)

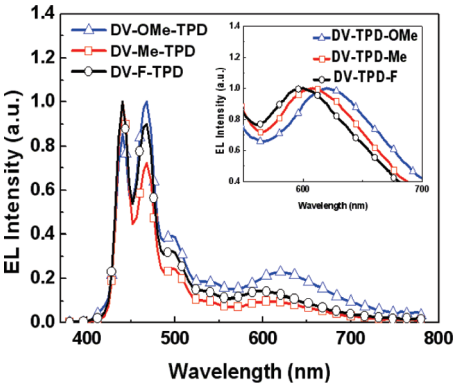

Figure 6. Electroluminescent spectra of the devices ITO/HTMs/PFO/CsF/Al at an applied potential of 11 V. Inset is the enlarged and normalized exciplex emission of the EL spectra.

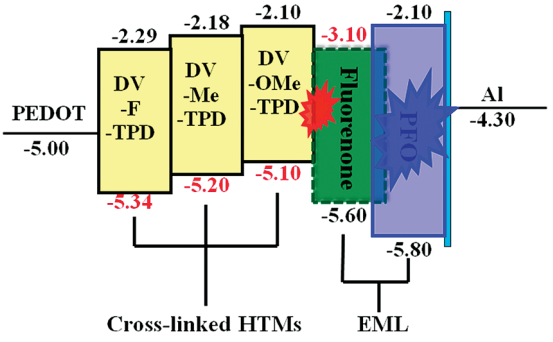

Figure 7. Red exciplex emission from HTM/fluorenone interface and blue exciton emission from PFO.

in **DV-OMe-TPD**-based device. This implies that the formation of fluorenone/**DV-OMe-TPD** exciplex at the interface is responsible for the red emission. Furthermore, when **DV-Me-TPD** and **DV-F-TPD** with the lower-lying HOMO energy levels are used to increase the energy gap at the interface, the emission maximum wavelength is shifted to 609 and 596 nm, respectively. The HOMO-dependent electroluminescence confirms the emission is derived from the exciplex emission. The energy diagram and the exciplex mechanism in the device are shown in Figure 7.

To further optimize the performance of **DV-Me-TPD**-based device, hole injection PEDOT:PSS was inserted in the device with the configuration of ITO/PEDOT:PSS/**DV-Me-TPD**/PFO/CsF/Al. Curing at a moderate temperature of 180 °C for 30 min allows for cross-linking of **DV-Me-TPD** layer without degrading the bottom PEDOT:PSS layer. As expected, the incorporation of PEDOT:PSS layer further enhances the device performance with a maximum luminance efficiency of 1.53 cd/A, maximum brightness of 3245 cd/m^2 and a lower turn-on voltage (Figures 4 and 5). The **DV-Me-TPD** layer has the HOMO levels at −5.2 eV, which is in between those of PEDOT:PSS (−5.0 eV) and PFO (−5.8 eV). Therefore, the PEDOT:PSS/**DV-Me-TPD** double layer provides an energy-matched cascade hole-injecting/transporting pathway leading to more balanced charge flux in the devices. The EL spectrum of PEDOT:PSS/**DV-Me-TPD**-based device also displays an exciplex emission, which is consistent with the devices without PEDOT:PSS layer.

Despite that the exciplex-induced red emission is detrimental to the PFO-based blue emitting devices, we envision that the dual

Table 3. Performance of the Devices ITO/PEDOT:PSS/DV-Me-TPD/PFO:*X* wt% BFBT/CsF/Al

BFBT (wt %)	B[a] (cd/m^2)	LE[a] (cd/A)	B_{max} (cd/m^2)	LE_{max} (cd/A)	CIE (x, y)[b]
0.02	570 (at 10.3 V)	2.90	4991 (at 18 V)	4.16	(0.25, 0.28)
0.04	619 (at 10.6 V)	3.11	3125 (at 17 V)	5.28	(0.32, 0.42)
0.08	672 (at 9.6 V)	3.49	4388 (at 16 V)	5.21	(0.32, 0.44)

[a] Recorded at 20 mA/cm^2. [b] Recorded at 9 V.

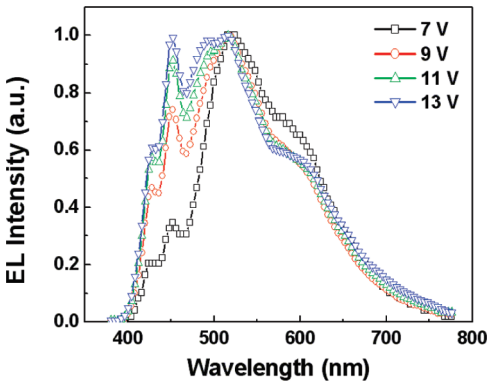

Figure 8. Electroluminescent spectra as a function of voltage for the device ITO/PEDOT:PSS/**DV-Me-TPD**/PFO:0.04 wt % **BFBT**/CsF/Al.

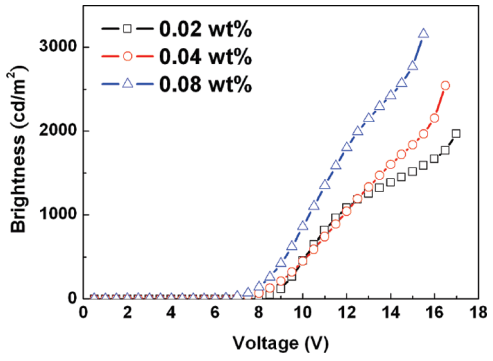

Figure 9. Brightness−voltage (B−V) characteristics based on the devices ITO/PEDOT:PSS/**DV-Me-TPD**/PFO:X wt % of **BFBT**/CsF/Al (X = 0.02, 0.04, and 0.08).

emission could be smartly utilized to realize white emitting PLED, if a green emitting source is incorporated in EML. In this regard, we fabricated the devices with the configuration ITO/PEDOT/**DV-Me-TPD**/PFO:X wt % of **BFBT**/CsF/Al where **BFBT** is a green emitting dopant in the emissive layer (Scheme 1). By doping small amount of **BFBT** (0.02, 0.04, and 0.08 wt %) to control energy transfer in the EML, the intensity of three primary colors can be carefully adjusted toward ideal white-light electroluminescence. Table 3 summarizes the characteristics of the white-emitting devices. Indeed, all the devices exhibited electroluminescence covering the entire visible window (400−800 nm) with three major peaks centered at ca. 450, 518, and 610 nm. The blue region is the characteristic emission of the PFO host, while the green and red emissions come from the **BFBT** dopant and the fluorenone/**DV-Me-TPD** exciplex, respectively. The Commission Internationale d'Énclairage (CIE) chromaticity coordinates were evaluated to determine the color

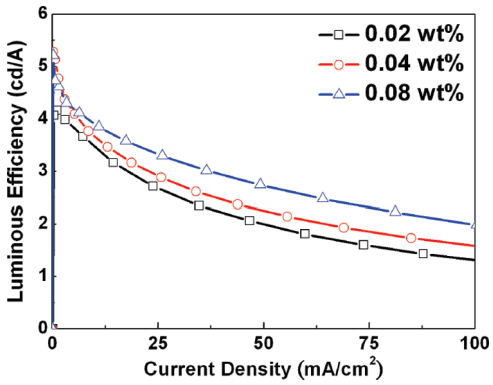

Figure 10. Luminous efficiency-current density characteristics based on the devices ITO/PEDOT:PSS/**DV-Me-TPD**/PFO:X wt % of **BFBT**/CsF/Al (X = 0.02, 0.04, and 0.08).

composition of the devices. The 0.02 wt % concentration of **BFBT** is too low to provide enough green light intensity. Thus, the corresponding device exhibited CIE chromaticity coordinates at (0.25, 0.28) at a bias of 9 V. However, by increasing the **BFBT** content, the CIE chromaticity coordinates were shifted to (0.32, 0.42) for the 0.04 wt % doped device and (0.32, 0.44) for 0.08 wt % doped device respectively, which are very close to the ideal white point (0.33, 0.33) (Figure 8). Figures 9 and 10 display the voltage−brightness (V−L) curves and luminous efficiency−current density of the white-emitting devices. As the doping content of **BFBT** increases from 0.02 to 0.04 and 0.08 wt %, the brightness and the luminous efficiency gradually increases, whereas the operation voltage is reduced. The 0.04 wt % doped white-emitting device showed a maximum luminance efficiency of 5.28 cd/A. To our knowledge, this value represents the highest among the exciplex-based white-emitting PLEDs.

CONCLUSIONS

Blue-emitting devices based on PFO suffer from poor color stability due to the formation of fluorenone defects. Utilization of fluorenone defects in PFO to induce exciplex emission may afford a useful strategy to achieve WPLED devices. Successful integration of triarylamine-based hole-transporting material into multilayer device plays a key role for exciplex formation at the HTL/EML interface. For this purpose, a new class of cross-linkable TPD-based HTMs, **DV-OMe-TPD**, **DV-Me-TPD**, and **DV-F-TPD**, were designed and synthesized. Two vinyl groups introduced on the two phenyl rings in the TPD unit are used as the cross-linkers, whereas methoxy, methyl and fluoro groups are incorporated to modulate the HOMO energy levels of the HTMs. After cross-linking under mild thermal polymerization, the HTL with solvent resistance can overcome interfacial mixing, allowing us to successfully fabricate the polyfluorene-based devices with configuration of ITO/cross-linked HTMs/PFO/CsF/Al.

In addition to the characteristic blue emission of PFO, the devices exhibited a red emission covering from 550 to 700 nm. The maximum wavelength of the red emission is correlated with the HOMO energy of the cross-linked HTM used in the device, suggesting that the red emission is derived from the exciplex formed by the adjacent hole and electron at the cross-linked HTM/fluorenone heterojunction interface. By doping small amounts of **BFBT** into EML to compensate green emission, the devices with the configuration of ITO/PEDOT/**DV-Me-TPD**/PFO doped with **BFBT**/CsF/Al) exhibited white electroluminescence comprising the three primary colors simultaneously. The 0.04 wt % doped device achieved a maximum luminous efficiency of 5.28 cd/A which represents the highest efficiency for WPLEDs based on the exciplex strategy. This device also showed CIE chromaticity coordinates of (0.32, 0.42) which are close to the ideal white point (0.33, 0.33).

EXPERIMENTAL SECTION

General Measurement and Characterization. All chemicals, unless we specified, were purchased from Aldrich, TCI, and Acros and used as received. The ^{1}H and ^{13}C NMR spectra were collected on a Varian Unity-300 spectrometer operating at 300 and 75 MHz in deuterated chloroform solution and using tetramethylsilane as reference. The IR spectra were collected using the PerkinElmer Spectrum One FT-IR spectrometer and these HTMs solution were dropped on the homemade KBr film for study. Cyclic voltammetric data were performed on a Autolab ADC 164 using a conventional three-electrode cell with an ITO glass as the working electrode, a platinum strip as the counter electrode, and a saturated calomel electrode as the reference electrode. 0.1 M (n-Bu$_4$)NBF$_4$ in acetonitrile is the electrolyte, and CV curves were calibrated using ferrocence as the standard, whose HOMO is −4.8 eV with respect to zero vacuum level. Differential scanning calorimetry (DSC) and thermal gravimetric analyzer (TGA) were measured on TA Q200 Instrument and Perkin-Elmer Pyris under a nitrogen atmosphere at a heating rate of 10 °C/min.

Device Fabrication. The patterned ITO glass substrates were ultrasonically cleaned with detergent, deionized water, acetone, and isopropyl alcohol. The PEDOT:PSS (Baytron P VP AI4083 from H. C. Stack) was spin-coated on the cleaned and UV-ozone treated ITO substrates. The PEDOT:PSS layer was baked at 120 °C for 30 min in air to remove residual water and then moved into a glovebox under nitrogen. The HTLs were formed by spin-coating (2000 rpm) the corresponding HTM solutions (1 wt % in chlorobenzene) onto ITO substrates or on top of the PEDOT:PSS layer and then thermally cross-linked on a hot plate at 180 °C for 30 min under nitrogen. Under this condition, we can generally obtain hole-transporting layers with ca. 25 nm thickness after cross-linking. The PFO solution (1 wt % in chlorobenzene) was spin-coated on top of the HTL(s) and then baked at 80 °C for 30 min under vacuum. Cesium fluoride (CsF) with the thickness of 2 nm and Al (100 nm) were thermally evaporated as cathode. The thickness of each layer in two device configurations is shown as the following: (1) ITO/HTL (∼25 nm)/PFO (∼70 nm)/CsF/Al; (2) ITO/PEDOT:PSS (∼40 nm)/HTL (∼25 nm)/PFO (∼70 nm)/CsF/Al. The current density−voltage-luminance characteristics of the devices were measured using an optical power meter PR-650 and a digital source meter Keithley 2400. The EL spectra were measured using a Photo Research PR-650 spectrophotometer under ambient condition after encapsulation.

Synthesis of 3a. To a two-necked flask were added Cu (10.34 g, 162.8 mmol), K_2CO_3 (22.5 g, 162.8 mmol), 18-crown-6 ether (200 mg), *N*,*N*′-diphenylbenzidine (**1**) (5 g, 14.8 mmol), 4-iodotoluene (**2a**) (9.7 g, 44.4 mmol), and *o*-dichlorobenzene (100 mL). The reaction mixture was stirred and heated at 190 °C under N_2 for 24 h. After filtration, the solvent was evaporated under reduced pressure. The residue was purified by column chromatography on silica gel (hexane/ethyl acetate, v/v, 20/1) to give a white solid, **3a** (6.34 g, 83%). ^{1}H NMR (300 MHz, $CDCl_3$): δ 2.32 (s, 6 H), 6.95−7.10 (m, 18 H), 7.20−7.24 (m, 4 H), 7.41 (d, J = 8.4 Hz, 4 H). ^{13}C NMR (75 MHz, $CDCl_3$):δ 21.1, 122.6, 123.8, 124.0, 125.3, 127.4, 129.4, 130.2, 133.1, 134.6, 145.4, 147.1, 148.1.

Synthesis of 4a. To a two-necked flask were added $POCl_3$ (1.76 g, 11.6 mmol) and DMF (0.85 g, 11.6 mmol) by syringe at 0 °C. The mixture was stirred at 0 °C for 30 min. **3a** (3 g, 5.8 mmol) dissolved in 1,2-dichloroethane (50 mL) was then added, and the reaction mixture was heated at 80 °C under N_2 for 6 h. After cooling to room temperature, the solution was quenched by NaOAc (aq) solution and stirred for 10 min. The mixture was extracted with CH_2Cl_2 and water to remove DMF. The solvent was removed by rotary evaporator. The residue was directly purified by column chromatography on silica gel (hexane/ethyl acetate, v/v, 6/1) to give a yellow solid **4a** (1.76 g, 53%). ^{1}H NMR (300 MHz, $CDCl_3$): δ 2.37 (s, 6 H), 7.05 (d, J = 8.4 Hz, 4 H), 7.10 (d, J = 8.4 Hz, 4 H), 7.17−7.23 (m, 8 H), 7.53 (d, J = 8.1 Hz, 4 H), 7.68 (d, J = 8.7 Hz, 4 H), 9.81 (s, 2 H). ^{13}C NMR (75 MHz, $CDCl_3$):δ 21.2, 119.5, 126.2, 126.9, 128.1, 129.3, 130.7, 131.6, 135.6, 136.7, 143.6, 145.7, 153.5, 190.6.

Synthesis of DV-Me-TPD. To a two-necked flask were added PPh_3CH_3Br (1.24 g, 3.5 mmol), NaH (0.084 g, 3.5 mmol) and dry THF (30 mL). The mixture was stirred at room temperature under N_2 for 1 h, followed by adding dry THF (20 mL) solution of **4a** (1 g, 1.7 mmol). The resulting reaction mixture was heated and stirred at 80 °C for 12 h. After cooling to room temperature, the solution was quenched by water and stirred for 5 min. The THF solvent was removed by rotary evaporator. The residue was extracted with ethyl acetate and water to remove the inorganic species. The organic layer was dried over $MgSO_4$. After removal of the solvent, the residue was directly purified by column chromatography on silica gel (hexane/ethyl acetate, v/v, 20/1) to give a white solid, **DV-Me-TPD** (0.38 g, 40%). ^{1}H NMR (300 MHz, $CDCl_3$): δ 2.33 (s, 6 H), 5.15 (d, J = 11.4 Hz, 2 H), 5.64 (d, J = 17.4, 2 H), 6.67 (dd, J_1 = 11.4 Hz, J_2 = 17.4 Hz, 2 H), 7.04 (d, J = 8.7 Hz, 8 H), 7.10 (d, J = 8.7 Hz, 8 H), 7.29 (d, J = 8.7 Hz, 4 H), 7.39−7.45 (m, 4 H). ^{13}C NMR (75 MHz, $CDCl_3$): δ 21.1, 122.2, 123.4, 124.1, 125.4, 127.3, 127.5, 130.2, 131.8, 133.4, 134.8, 136.5, 145.1, 146.8, 147.7. MS (FAB−MS) m/z: 569. Anal. Calcd for $C_{42}H_{36}N_2$: C, 88.69 ; H, 6.38 ; N, 4.93. Found: C, 88.46 ; H, 6.41 ; N, 5.08.

Synthesis of 3b. To a two-necked flask were added Cu (10.34 g, 162.8 mmol), K_2CO_3 (22.5 g, 162.8 mmol), 18-crown-6 ether (200 mg), *N*,*N*′-diphenylbenzidine (**1**) (5 g, 14.8 mmol), 4-iodoanisole (**2b**) (10.4 g, 44.4 mmol) and *o*-dichlorobenzene (100 mL). The reaction mixture was stirred and heated at 190 °C under N_2 for 24 h. The hot mixture solution was filtered, and the solution was evaporated under reduced pressure. The residue was purified by column chromatography on silica gel (hexane/ethyl acetate, v/v, 20/1) to give a white solid **3b** (6.89 g, 85%). ^{1}H NMR (300 MHz, $CDCl_3$): δ 3.79 (s, 6 H), 6.84 (d, J = 9 Hz, 4 H), 6.95 (t, J = 6.9 Hz, 2 H), 7.04−7.11 (m, 12 H), 7.19−7.24 (m, 4 H), 7.40 (d, J = 8.4 Hz, 4 H). ^{13}C NMR (75 MHz, $CDCl_3$): δ 55.7, 115.0, 122.2, 123.1, 123.3, 127.4, 127.6, 129.4, 134.3, 140.9, 147.2, 148.3, 156.4. MS (FAB−MS) m/z: 549.

Synthesis of 4b. To a two-necked flask were added $POCl_3$ (1.65 g, 10.8 mmol) and DMF (0.79 g, 10.8 mmol) by syringe at 0 °C. The mixture was stirred at 0 °C for 30 min. **3b** (3 g, 5.4 mmol) dissolved in 1,2-dichloroethane (50 mL) was then added, and the reaction mixture was heated at 80 °C under N_2 for 6 h. After cooling to room temperature, the solution was quenched by NaOAc solution and stirred for 10 min. The mixture was extracted with CH_2Cl_2 and water to remove DMF. The solvent was removed by rotary evaporator. The residue was directly purified by column chromatography on silica gel (hexane/ethyl acetate, v/v, 6/1) to give a yellow solid, **4b** (1.95 g, 60%). ^{1}H NMR (300 MHz, $CDCl_3$): δ 3.83 (s, 6 H), 6.92 (d, J = 9 Hz, 4 H), 7.01 (d, J = 9 Hz, 4 H),

7.14−7.23 (m, 8 H), 7.52(d, J = 8.7 Hz, 4 H), 7.18 (d, J = 8.7 Hz, 4 H), 9.80 (s, 2 H). ^{13}C NMR (75 MHz, $CDCl_3$): δ 55.5, 115.2, 118.6, 125.7, 127.8, 128.5, 128.8, 131.4, 136.4, 138.7, 145.4, 153.4, 157.6, 190.4. MS (FAB−MS) m/z: 604.

Synthesis of DV-OMe-TPD. To a two-necked flask were added PPh_3CH_3Br (1.18 g, 3.3 mmol), NaH (0.079 g, 3.3 mmol) and dry THF (30 mL). The mixture was stirred at room temperature under N_2 for 1 h, followed by adding **4b** (1 g, 1.6 mmol) solution of dry THF (20 mL). The resulting reaction mixture was heated and stirred at 80 °C for 12 h. After cooling to room temperature, the solution was quenched by water and stirred for 5 min. The THF solvent was removed by rotary evaporator. The residue was extracted with ethyl acetate and water to remove the inorganic species. The organic layer was dried over $MgSO_4$. After removal of the solvent, the residue was directly purified by column chromatography on silica gel (hexane/ethyl acetate, v/v, 20/1) to give a white solid, **DV-OMe-TPD** (0.47 g, 49%). ^{1}H NMR (300 MHz, $CDCl_3$): δ 3.81 (s, 6 H), 5.13 (d, J = 10.8 Hz, 2 H), 5.62 (d, J = 17.4 Hz), 6.65 (d, J_1 = 10.8 Hz, J_2 = 17.4 Hz, 2 H), 6.86 (d, J = 15.9 Hz, 4 H), 7.00−7.13 (m, 16 H), 7.27 (d, J = 9.9 Hz, 4 H), 7.41 (d, J = 9 Hz, 4 H). ^{13}C NMR (75 MHz, $CDCl_3$): δ 55.5, 111.8, 114.8, 122.5, 123.2, 127.0, 127.2, 127.4, 131.2, 134.3, 136.2, 140.4, 146.7, 147.6, 156.3. MS (FAB−MS) m/z: 601. Anal. Calcd for $C_{42}H_{36}N_2O_2$: C, 83.97; H, 6.04; N, 4.66. Found: C, 83.62; H, 6.31; N, 4.78.

Synthesis of 3c. $Pd_2(dba)_3$ (0.6 g, 0.66 mmol) and tri-*tert*-butylphosphane (0.8 g, 4 mmol) were dissolved in dry toluene (20 mL) under N_2 and the solution was stirred for 10 min at room temperature. The mixture was added to the toluene solution containing *N*,*N*′-diphenylbenzidine (**1**) (5 g, 14.8 mmol), 4-fluoroiodobenzene (**2c**) (6.5 g, 29.6 mmol), and *t*-BuONa (3.5 g, 37 mmol). The solution was degassed with N_2 for 20 min and then was heated at 100 °C for 20 h. The hot mixture solution was filtered, and the solvent was removed in vacuo. The residue was purified by column chromatography on silica gel (hexane/ethyl acetate, v/v, 20/1) to give a white solid, **3c** (6.8 g, 87%). ^{1}H NMR (300 MHz, $CDCl_3$):δ 7.06−7.25 (m, 18 H), 7.34−7.40 (m, 4 H), 7.53−7.56 (m, 4 H).

Synthesis of 4c. To a two-necked flask were added $POCl_3$ (1.75 g, 11.4 mmol) and DMF (0.83 g, 11.4 mmol) by syringe at 0 °C. The mixture was stirred at 0 °C for 30 min. **3c** (3 g, 5.7 mmol) dissolved in 1,2-dichloroethane (50 mL) was then added, and the reaction mixture was heated at 80 °C under N_2 for 6 h. After cooling to room temperature, the solution was quenched by NaOAc solution and stirred for 10 min. The mixture was extracted with CH_2Cl_2 and water to remove DMF. The solvent was removed by rotary evaporator. The residue was directly purified by column chromatography on silica gel (hexane/ethyl acetate, v/v, 6/1) to give a yellow solid **4c** (1.80 g, 54%). ^{1}H NMR (300 MHz, $CDCl_3$): δ 7.03−7.10 (m, 8 H), 7.17−7.26 (m, 8 H), 7.54 (d, J = 8.4 Hz, 4 H), 7.71 (d, J = 8.4 Hz, 4 H), 9.82 (s, 2 H). ^{13}C NMR (75 MHz, $CDCl_3$): δ 116.6, 116.9, 119.4, 125.9, 128.0, 128.3, 128.4, 129.4, 131.4, 136.6, 142.0, 142.0, 145.3, 153.1, 158.6, 161.8, 190.4. MS (EI−MS) m/z: 581.

Synthesis of DV-F-TPD. To a two-necked flask were added PPh_3CH_3Br (1.23 g, 3.4 mmol), NaH (0.08 g, 3.4 mmol), and dry THF (30 mL). The mixture was stirred at room temperature under N_2 for 1 h, followed by adding **4c** (1 g, 1.72 mmol) solution of dry THF (20 mL). The resulting reaction mixture was heated and stirred at 80 °C for 12 h. After cooling to room temperature, the solution was quenched by water and stirred for 5 min. The THF solvent was removed by rotary evaporator. The residue was extracted with ethyl acetate and water to remove the inorganic species. The organic layer was dried over $MgSO_4$. After removal of the solvent, the residue was directly purified by column chromatography on silica gel (hexane/ethyl acetate, v/v, 20/1) to give a white solid **DV-F-TPD** (0.38 g, 38%). ^{1}H NMR (300 MHz, $CDCl_3$): δ 5.17 (d, J = 10.8 Hz, 2 H), 5.65 (d, J = 17.4 Hz, 2 H), 6.67 (dd, J_1 = 10.8 Hz, J_2 = 17.4 Hz, 2 H), 6.96−7.14 (m, 16 H), 7.31 (d, J = 8.4 Hz, 4 H), 7.42−7.46 (m, 4 H). ^{13}C NMR (75 MHz, $CDCl_3$): δ 112.5, 116.3, 116.6, 123.5, 123.9, 126.9, 127.0, 127.4, 127.6, 132.2, 135.0, 136.4, 143.7, 146.8, 147.5. MS (FAB−MS) m/z: 577. Anal. Calcd for $C_{40}H_{30}F_2N_2$: C, 83.31; H, 5.24; N, 4.89. Found: C, 82.73; H, 5.86; N, 4.91.

■ ASSOCIATED CONTENT

Supporting Information. Absorption spectra, IR spectra, AFM images, and NMR spectra of the new compounds. This material is available free of charge via the Internet at http://pubs.acs.org.

■ AUTHOR INFORMATION

Corresponding Author
*E-mail: yjcheng@mail.nctu.edu.tw.

■ ACKNOWLEDGMENT

This work is supported by the National Science Council and "ATU Plan" of the National Chiao Tung University and Ministry of Education, Taiwan.

■ REFERENCES

(1) (a) D'Andrade, B. W.; Forrest, S. R. *Adv. Mater.* **2004**, *16*, 1585. (b) Kido, J.; Kimura, M.; Nagai, K. *Science* **1995**, *267*, 1332. (c) Wu, H.; Ying, L.; Yang, W.; Cao, Y. *Chem. Soc. Rev.* **2009**, *38*, 3391.

(2) (a) Gustafsson, G.; Cao, Y.; Treacy, G. M.; Klavetter, F.; Colaneri, N.; Heeger, A. J. *Nature* **1992**, *357*, 477. (b) Zhang, Y.; Huang, F.; Chi, Y.; Jen, A. K. Y. *Adv. Mater.* **2008**, *20*, 1565. (c) Wu, H.; Zou, J.; Liu, F.; Wang, L.; Mikhailovsky, A.; Bazan, G. C.; Yang, W.; Cao, Y. *Adv. Mater.* **2008**, *20*, 696.

(3) (a) Berggren, M.; Inganas, O.; Gustafsson, G.; Rasmusson, J.; Andersson, M. R.; Hjertberg, T.; Wennerstrom, O. *Nature* **1994**, *372*, 444. (b) Tasch, S.; List, E. J. W.; Ekstrom, O.; Graupner, W.; Leising, G.; Schlichting, P.; Rohr, U.; Geerts, Y.; Scherf, U.; Mullen, K. *Appl. Phys. Lett.* **1997**, *71*, 2883. (c) Huang, J.; Li, G.; Wu, E.; Xu, Q.; Yang, Y. *Adv. Mater.* **2006**, *18*, 114.

(4) (a) Xu, Y.; Peng, J.; Jiang, J.; Xu, W.; Yang, W.; Cao, Y. *Appl. Phys. Lett.* **2005**, *87*, 193502. (b) Kido, J.; Shionoya, H.; Nagai, K. *Appl. Phys. Lett.* **1995**, *67*, 2281. (c) Kim, J. H.; Herguth, P.; Kang, M.-S.; Jen, A. K. Y.; Tseng, Y.-H.; Shu, C.-F. *Appl. Phys. Lett.* **2004**, *85*, 1116. (d) Gong, X.; Ma, W.; Ostrowski, J. C.; Bazan, G. C.; Moses, D.; Heeger, A. J. *Adv. Mater.* **2004**, *16*, 615. (e) Xu, Q.; Duong, H. M.; Wudl, F.; Yang, Y. *Appl. Phys. Lett.* **2004**, *85*, 3357.

(5) Xia, Y.; Friend, R. H. *Adv. Mater.* **2006**, *18*, 1371.

(6) (a) Tu, G.; Zhou, Q.; Cheng, Y.; Wang, L.; Ma, D.; Jing, X.; Wang, F. *Appl. Phys. Lett.* **2004**, *85*, 2172. (b) Paik, K. L.; Baek, N. S.; Kim, H. K.; Lee, J.-H.; Lee, Y. *Macromolecules* **2002**, *35*, 6782. (c) Chuang, C.-Y.; Shih, P.-I.; Chien, C.-H.; Wu, F.-I.; Shu, C.-F. *Macromolecules* **2007**, *40*, 247. (d) Liu, J.; Zhou, Q.; Cheng, Y.; Geng, Y.; Wang, L.; Ma, D.; Jing, X.; Wang, F. *Adv. Mater.* **2005**, *17*, 2974. (e) Lee, S. K.; Hwang, D.-H.; Jung, B.-J.; Cho, N. S.; Lee, J.; Lee, J.-D.; Shim, H.-K. *Adv. Funct. Mater.* **2005**, *15*, 1647. (f) Wu, W.-C.; Lee, W.-Y.; Chen, W.-C. *Macromol. Chem. Phys.* **2006**, *207*, 1131. (g) Liu, J.; Xie, Z.; Cheng, Y.; Geng, Y.; Wang, L.; Jing, X.; Wang, F. *Adv. Mater.* **2007**, *19*, 531. (h) Jiang, J.; Xu, Y.; Yang, W.; Guan, R.; Liu, Z.; Zhen, H.; Cao, Y. *Adv. Mater.* **2006**, *18*, 1769.

(7) (a) Loy, D. E.; Koene, B. E.; Thompson, M. E. *Adv. Funct. Mater.* **2002**, *12*, 245. (b) Tanaka, H.; Tokito, S.; Taga, Y.; Okada, A. *Chem. Commun.* **1996**, 2175. (c) Shirota, Y. *J. Mater. Chem.* **2000**, *10*, 1. (d) Adachi, C.; Nagai, K.; Tamoto, N. *Appl. Phys. Lett.* **1995**, *66*, 2679. (e) Li, J.; Ma, C.; Tang, J.; Lee, C.-S.; Lee, S. *Chem. Mater.* **2005**, *17*, 615. (f) Liao, Y.-L.; Hung, W.-Y.; Hou, T.-H.; Lin, C.-Y.; Wong, K.-T. *Chem. Mater.* **2007**, *19*, 6350.

(8) (a) Morteani, A. C.; Dhoot, A. S.; Kim, J.-S.; Silva, C.; Greenham, N. C.; Murphy, C.; Moons, E.; Cina, S.; Burroughes, J. H.; Friend, R. H. *Adv. Mater.* **2003**, *15*, 1708. (b) Morteani, A. C.; Ho, P. K. H.; Friend, R. H.; Silva, C. *Appl. Phys. Lett.* **2005**, *86*, 163501. (c) Sun, Q. J.; Fan, B. H.; Tan, Z. A.; Yang, C. H.; Li, Y. F.; Yang, Y. *Appl. Phys. Lett.* **2006**, *88*, 163510. (d) Holmes, R. J.; D'Andrade, B. W.; Forrest, S. R.; Ren, X.; Li, J.; Thompson, M. E. *Appl. Phys. Lett.* **2003**, *83*, 3818. (e) Feng, J.; Li, F.; Gao, W.; Liu, S.; Liu, Y.; Wang, Y. *Appl. Phys. Lett.* **2001**, *78*, 3947. (f) Matsumoto, N.; Nishiyama, M.; Adachi, C. *J. Phys. Chem. C* **2008**, *112*, 7735. (g) Gebler, D. D.; Wang, Y. Z.; Blatchford, J. W.; Jessen, S. W.; Fu, D.-K.; Swager, T. M.; MacDiarmid, A. G.; Epstein, A. J. *Appl. Phys. Lett.* **2001**, *70*, 1644. (h) Jiang, X.; Liu, M. S.; Jen, A. K. Y. *J. Appl. Phys.* **2002**, *91*, 10147.

(9) (a) Liu, S.; Jiang, X.; Ma, H.; Liu, M. S.; Jen, A. K. Y. *Macromolecules* **2000**, *33*, 3514. (b) Bacher, E.; Bayerl, M.; Rudati, P.; Reckefuss, N.; Mueller, C. D.; Meerholz, K.; Nuyken, O. *Macromolecules* **2005**, *38*, 1640. (c) Domercq, B.; Hreha, R. D.; Zhang, Y.-D.; Larribeau, N.; Haddock, J. N.; Schultz, C.; Marder, S. R.; Kippelen, B. *Chem. Mater.* **2003**, *15*, 1491. (d) Zacharias, P.; Gather, M. C.; Rojahn, M.; Nuyken, O.; Meerholz, K. *Angew. Chem., Int. Ed.* **2007**, *46*, 4388. (e) Yang, X.; Muller, D. C.; Neher, D.; Meerholz, K. *Adv. Mater.* **2006**, *18*, 948. (f) Muller, C. D.; Falcou, A.; Reckefuss, N.; Rojahn, M.; Wiederhirn, V.; Rudati, P.; Frohne, H.; Nuyken, O.; Bechker, H.; Meerholz, K. *Nature* **2003**, *421*, 829. (g) Jenekhe, S. A.; Osaheni, J. A. *Science* **1994**, *265*, 765.

(10) Chao, C.-I.; Chen, S.-A. *Appl. Phys. Lett.* **1998**, *73*, 426.

(11) (a) Chen, Q.; Liu, N.; Ying, L.; Yang, W.; Wu, H.; Xu, W.; Cao., Y. *Polymer.* **2009**, *50*, 1430. (b) Yang, R.; Tian, R.; Yan, J.; Zhang, Y.; Yang, J.; Hou, Q.; Yang, W.; Zhang, C.; Cao, Y. *Macromolecules* **2005**, *38*, 244. (c) Yang, R.; Tian, R.; Hou, Q.; Yang, W.; Cao, Y. *Macromolecules* **2003**, *36*, 7453.

(12) (a) Cheng, Y.-J.; Liu, M. S.; Zhang, Y.; Niu, Y.; Huang, F.; Ka, J.-W.; Yip, H.-L.; Tian, Y.; Jen, A. K. Y. *Chem. Mater.* **2008**, *20*, 413. (b) Niu, Y.-H.; Munro, A. M.; Cheng, Y.-J.; Tian, Y.; Liu, M. S.; Zhao, J.; Bardecker, J. A.; Plante, I. J.-L.; Ginger, D. S.; Jen, A. K. Y. *Adv. Mater.* **2007**, *19*, 3371. (c) Niu, Y.-H.; Liu, M. S.; Ka, J.-W.; Bardeker, J.; Zin, M. T.; Schofield, R.; Chi, Y.; Jen, A. K. Y. *Adv. Mater.* **2007**, *19*, 300. (d) Liu, M. S.; Niu, Y.-H.; Ka, J.-W.; Yip, H.-L.; Huang, F.; Luo, J.; Kim, T.-D.; Jen, A. K. Y. *Macromolecules* **2008**, *41*, 9570. (e) Huang, F.; Cheng, Y.-J.; Zhang, Y.; Liu, M. S.; Jen, A. K.-Y. *J. Mater. Chem.* **2008**, *18*, 4485. (f) Zuniga, C. A.; Barlow, S.; Marder, S. R. *Chem. Mater.* **2011**, *23*, 658.

(13) (a) O'Brien, D. F.; Burrows, P. E.; Forrest, S. R.; Koene, B. E.; Loy, D. E.; Thompson, M. E. *Adv. Mater.* **1998**, *10*, 1108. (b) Hreha, R. D.; George, C. P.; Haldi, A.; Domercq, B.; Malagoli, M.; Barlow, S.; Brédas, J.-L.; Kippelen, B.; Marder, S. R. *Adv. Funct. Mater.* **2003**, *13*, 967. (c) Bach, U.; De, C. K.; Spreitzer, H.; Gratzel, M. *Adv. Mater.* **2000**, *12*, 1060.

(14) (a) Khuong, K. S.; Jones, W. H.; Pryor, W. A.; Houk, K. N. *J. Am. Chem. Soc.* **2005**, *127*, 1265. (b) Mayo, F. *J. Am. Chem. Soc.* **1968**, *90*, 1289. (c) Chong, Y. K.; Rizzardo, E.; Solomon, D. H. *J. Am. Chem. Soc.* **1983**, *105*, 7761.

(15) (a) Scherf, U.; List, E. J. W. *Adv. Mater.* **2002**, *14*, 477. (b) Pei, Q.; Yang, Y. *J. Am. Chem. Soc.* **1996**, *118*, 7416. (c) Yang, Y.; Pei, Q. *J. Appl. Phys.* **1997**, *81*, 3294. (d) Kreyenschmidt, M.; Klaerner, G.; Fuhrer, T.; Ashenhurst, J.; Karg, S.; Chen, W. D.; Lee, V. Y.; Scott, J. C.; Miller, R. D. *Macromolecules* **1998**, *31*, 1099. (e) Ranger, M.; Rondeau, D.; Leclerc, M. *Macromolecules* **1997**, *30*, 7686. (f) Marsitzky, D.; Vestberg, R.; Blainey, P.; Tang, B. T.; Hawker, C. J.; Carter, K. R. *J. Am. Chem. Soc.* **2001**, *123*, 6965. (g) Xia, C.; Advincula, R. C. *Macromolecules* **2001**, *34*, 5854.

(16) (a) Gong, X.; Iyer, P. K.; Moses, D.; Bazan, G. C.; Heeger, A. J.; Xiao, S. S. *Adv. Funct. Mater.* **2003**, *13*, 325. (b) Bliznyuk, V. N.; Carter, S. A.; Scott, J. C.; Klaerner, G.; Miller, R. D.; Miller, D. C. *Macromolecules* **1999**, *32*, 361. (c) Uckert, F.; Tak, Y.-H.; Müllen, K.; Bassler, H. *Adv. Mater.* **2000**, *12*, 905. (d) List, E. J. W.; Guentner, R.; Scanducci, d. F. P.; Scherf, U. *Adv. Mater.* **2002**, *14*, 374. (e) Craig, M. R.; de, K. M. M.; Hofstraat, J. W.; Schenning, A. P. H. J.; Meijer, E. W. *J. Mater. Chem.* **2003**, *13*, 2861. (f) Gaal, M.; List, E. J. W.; Scherf, U. *Macromolecules* **2003**, *36*, 4236. (g) Surin, M.; Hennebicq, E.; Ego, C.; Marsitzky, D.; Grimsdale, A. C.; Müllen, K.; Brédas, J.-L.; Lazzaroni, R.; Leclere, P. *Chem. Mater.* **2004**, *16*, 994.

(17) (a) Gong, X.; Moses, D.; Heeger, A. J.; Xiao, S. *Synth. Met.* **2004**, *141*, 17. (b) Gong, X.; Moses, D.; Heeger, A. J.; Xiao, S. *J. Phys. Chem. B* **2004**, *108*, 8601. (c) Sun, Q. J.; Fan, B. H.; Tan, Z. A.; Yang, C. H.; Li, Y. F.; Yang, Y. *Appl. Phys. Lett.* **2006**, *88*, 163510/1.